U.S. ARMY

RESEARCH LABORATORY

Stabilizing Gyroscopic Modes in Magnetic-Bearing-Supported Flywheels by Using Cross-Axis Proportional Gains

Gerald V. Brown
Glenn Research Center, Cleveland, Ohio

Albert F. Kascak
U.S. Army Research Laboratory, Glenn Research Center, Cleveland, Ohio

Ralph H. Jansen
University of Toledo, Toledo, Ohio

Timothy P. Dever
QSS Group, Inc., Cleveland, Ohio

Kirsten P. Duffy
University of Toledo, Toledo, Ohio

January 2006

The NASA STI Program Office . . . in Profile

Since its founding, NASA has been dedicated to the advancement of aeronautics and space science. The NASA Scientific and Technical Information (STI) Program Office plays a key part in helping NASA maintain this important role.

The NASA STI Program Office is operated by Langley Research Center, the Lead Center for NASA's scientific and technical information. The NASA STI Program Office provides access to the NASA STI Database, the largest collection of aeronautical and space science STI in the world. The Program Office is also NASA's institutional mechanism for disseminating the results of its research and development activities. These results are published by NASA in the NASA STI Report Series, which includes the following report types:

- TECHNICAL PUBLICATION. Reports of completed research or a major significant phase of research that present the results of NASA programs and include extensive data or theoretical analysis. Includes compilations of significant scientific and technical data and information deemed to be of continuing reference value. NASA's counterpart of peer-reviewed formal professional papers but has less stringent limitations on manuscript length and extent of graphic presentations.

- TECHNICAL MEMORANDUM. Scientific and technical findings that are preliminary or of specialized interest, e.g., quick release reports, working papers, and bibliographies that contain minimal annotation. Does not contain extensive analysis.

- CONTRACTOR REPORT. Scientific and technical findings by NASA-sponsored contractors and grantees.

- CONFERENCE PUBLICATION. Collected papers from scientific and technical conferences, symposia, seminars, or other meetings sponsored or cosponsored by NASA.

- SPECIAL PUBLICATION. Scientific, technical, or historical information from NASA programs, projects, and missions, often concerned with subjects having substantial public interest.

- TECHNICAL TRANSLATION. English-language translations of foreign scientific and technical material pertinent to NASA's mission.

Specialized services that complement the STI Program Office's diverse offerings include creating custom thesauri, building customized databases, organizing and publishing research results . . . even providing videos.

For more information about the NASA STI Program Office, see the following:

- Access the NASA STI Program Home Page at *http://www.sti.nasa.gov*

- E-mail your question via the Internet to help@sti.nasa.gov

- Fax your question to the NASA Access Help Desk at 301–621–0134

- Telephone the NASA Access Help Desk at 301–621–0390

- Write to:
  NASA Access Help Desk
  NASA Center for AeroSpace Information
  7121 Standard Drive
  Hanover, MD 21076

Stabilizing Gyroscopic Modes in Magnetic-Bearing-Supported Flywheels by Using Cross-Axis Proportional Gains

Gerald V. Brown
Glenn Research Center, Cleveland, Ohio

Albert F. Kascak
U.S. Army Research Laboratory, Glenn Research Center, Cleveland, Ohio

Ralph H. Jansen
University of Toledo, Toledo, Ohio

Timothy P. Dever
QSS Group, Inc., Cleveland, Ohio

Kirsten P. Duffy
University of Toledo, Toledo, Ohio

National Aeronautics and
Space Administration

Glenn Research Center

January 2006

Stabilizing Gyroscopic Modes in Magnetic-Bearing-Supported Flywheels by Using Cross-Axis Proportional Gains

Gerald V. Brown
National Aeronautics and Space Administration
Glenn Research Center
Cleveland, Ohio 44135

Albert F. Kascak
U.S. Army Research Laboratory
Glenn Research Center
Cleveland, Ohio 44135

Ralph H. Jansen
University of Toledo
Toledo, Ohio 43606

Timothy P. Dever
QSS Group, Inc.
Cleveland, Ohio 44135

Kirsten P. Duffy
University of Toledo
Toledo, Ohio 43606

Abstract

For magnetic-bearing-supported high-speed rotating machines with significant gyroscopic effects, it is necessary to stabilize forward and backward tilt whirling modes. Instability or low damping of these modes can prevent the attainment of desired shaft speed. We show analytically that both modes can be stabilized by using cross-axis proportional gains and high- and low-pass filters in the magnetic bearing controller. Furthermore, at high shaft speeds, where system phase lags degrade the stability of the forward-whirl mode, a phasor advance of the control signal can partially counteract the phase lag. In some range of high shaft speed, the derivative gain for the tilt modes (essential for stability for slowly rotating shafts) can be removed entirely. We show analytically how the tilt eigenvalues depend on shaft speed and on various controller feedback parameters.

Nomenclature

f	effective filter approximately representing all system filters
g_b	cross-axis gain for stabilizing backward whirl
g_{ca}	general cross-axis gain
g_f	cross-axis gain for stabilizing forward whirl
I_p	shaft polar moment of inertia
I_t	shaft transverse moment of inertia
r	complex tilt displacement
ω_0	tilt frequency for non-spinning shaft
ω_c	corner frequency of assumed filters
λ	complex tilt eigenvalue
ζ	damping constant for tilt motion
Ω	adjusted non-dimensionalized shaft speed $\equiv \Omega' (I_p/I_t)/\omega_0$
Ω'	shaft spinning speed
Ω_0	reference shaft adjusted speed for zeta reduction

I. Introduction and Approach

High-speed flywheels are being considered for a variety of earth and space applications that require energy storage or attitude control. For long life and low energy loss at very high speeds, magnetic bearing support of the flywheels is preferred. However, these flywheels exhibit highly gyroscopic behavior which presents magnetic bearing control problems that do not arise for shafts with very small polar moments of inertia. We discuss approaches to the control of the gyroscopic modes that avoid high control effort and are simple to implement and understand.

We consider only a rigid shaft and treat it as a free body, acted upon by external forces applied by two radial magnetic bearings and by the internally-generated gyroscopic torques. The axial degree of freedom is assumed to be controlled by an axial magnetic bearing and is ignored. The negative stiffness of linearized magnetic bearings is usually treated as part of the plant model. But to attain a "free body" treatment of the shaft, we presume that the negative stiffness is first nullified by appropriate proportional gains in the magnetic bearing controller. Then the normal modes of the shaft are pure center-of-mass translations and pure tilts about the center of mass. Hence we can use a centralized, modal-control approach that treats the rotor's tilt and center-of-mass-translation modes independently. Control of the center-of-mass translation modes does not present any problems, and only the tilt modes exhibit speed-dependent gyroscopic effects. Consequently we treat only the tilt modes in this paper.

The motivation to use cross-axis proportional gains stems from a desire to avoid the increase in noise and control effort associated with same-axis derivative gains or with cross-axis derivative gains, the latter of which arise in gyroscopic-cancellation techniques (ref. 1). In a conventional PID magnetic bearing controller, the shaft displacement is differentiated to get the shaft velocity so that the actuator can oppose that velocity and hence damp vibration. (Obtaining the velocity by differentiation or from an observer controller is required because velocity is rarely actually measured.) Extra derivative gain is required to counteract control system phase lags at high frequencies. But because of the special whirling nature of gyroscopic modes, it is possible to obtain the tilt velocities without differentiation. In a pure whirl mode the shaft tilt velocity in one plane is equal (to within a sign) to the tilt displacement in the perpendicular plane times the mode frequency. Since both displacements are always being measured, it would appear that differentiation can be avoided entirely. This would be straightforward to implement for a single whirl direction, but the sign of the required gain is opposite for the two whirling directions. The cross-axis proportional gain that stabilizes forward-whirl destabilizes backward whirl and vice versa.

The key to controlling both tilt modes at high shaft speeds is to utilize the considerable difference in their frequencies that develops at higher shaft speed. The forward-whirl mode frequency is asymptotic to $(I_p/I_t)* \ \Omega'$, where Ω' is the shaft angular speed and I_p and I_t are the shaft polar and transverse moments of inertia. The frequency of the backward-whirl mode is approximately inversely proportional to that of the forward-whirl. The mode frequencies can differ by more than two orders of magnitude in high-speed flywheels. We can therefore utilize two parallel paths through the controller which are separated by low- and high-pass filters. One path, containing a low-pass filter, stabilizes the backward-whirl tilt mode with an appropriately-signed cross-axis proportional gain. The other path, containing a high-pass filter and an oppositely-signed cross-axis gain, stabilizes the forward-whirl mode. We therefore achieve very independent action on the two whirl modes at high shaft speed. Because the physical gyroscopic torques are proportional to the spinning speed of the shaft, it is convenient to gain-schedule the cross-axis control terms by making them proportional to shaft speed.

Phase lags in the closed control loop place a limit on the shaft speed at which the above simple method is sufficient. The forward-whirl mode frequency can become high enough that the system phase lags are appreciable. Hence that mode's stability is degraded and eventually lost as shaft speed increases. (The lags come from the finite bandwidths of power amplifiers, position sensors, anti-alias and smoothing filters, as well as from controller sampling rate and latency and magnetic bearing core eddy currents.) In order to maintain stability to higher speed the frequency of the forward-whirl mode and the phase lags at that frequency can be measured or estimated as a function of shaft speed. With this information a "phasor" lead can be introduced to extend the benefits of cross-axis proportional gains to much higher shaft speeds. At a given shaft speed the tilt displacements in two planes can be expressed as a single complex "phasor" displacement. The control output can also be expressed as a complex phasor. The effect of the total system phase lag θ (at the forward-whirl frequency) on the complex control force is simply to multiply the intended force by $\exp(-i\theta)$. The effect of the lag would be nullified if the control output command is multiplied by $\exp(i\theta)$. Any smaller phasor advance that might be applied is better than none. In some range of high shaft speed, the derivative gain for the tilt modes (essential for stability for slowly rotating shafts) can be removed entirely.

II. Analysis and Results

A. Infinite Bandwidth without Cross-Axis Gains

Let the tilt angular displacements in the two perpendicular planes through the non-displaced shaft axis be designated by the real and imaginary parts of a complex variable r. Then the governing differential equation of shaft tilt motion, with only proportional and derivative feedback in the magnetic bearing controller and for infinite closed-loop bandwidth, is (in agreement with the axes and sign conventions of refs. 2 and 3)

$$d^2r/dt^2 + i\Omega'\left(I_p/I_t\right)dr/dt + 2\zeta\omega_0\,dr/dt + \omega_0^2 r = 0 \qquad (1)$$

where Ω' is the shaft angular rotation speed, r is the complex tilt displacement, ω_0 is the tilt frequency for the non-rotating shaft and ζ is the tilt damping factor for the non-rotating shaft. (Note that the terms after the first two arise from magnetic bearing action; ω_0 and ζ are determined by the proportional and derivative gains in the magnetic bearing control law, as well as by I_p/I_t.) The characteristic equation for the complex tilt eigenvalue λ', obtained by assuming solutions of the form $r = A \exp(\lambda' t)$, is

$$\lambda'^2 + i\Omega'\left(I_p/I_t\right)\lambda' + 2\zeta\omega_0\lambda' + \omega_0^2 = 0 \qquad (2)$$

The imaginary part of λ' is the modal angular frequency and the real part is the absolute growth rate (negative of damping) for the mode. It is convenient to non-dimensionalize by dividing each term of equation (2) by ω_0^2, yielding

$$\lambda^2 + i\Omega\lambda + 2\zeta\lambda + 1 = 0 \qquad (3)$$

where $\lambda = \lambda'/\omega_0$ and $\Omega \equiv \Omega'\,(I_p/I_t)/\omega_0$. Thus all frequencies are measured in units of the non-spinning tilt frequency ω_0, which is set by the proportional gain in the magnetic bearing controller. The negative of the real part of the eigenvalue, divided by ω_0, is analogous to the damping factor ζ. The frequency ω_0 may typically be on the order of 2π times 50 Hz, as was roughly the case for the flywheel in reference 4. Equation (1) and subsequent characteristic equations were solved numerically for the eigenvalues by using commercial software. The two nondimensional eigenvalues, $\lambda+$ with positive frequency (forward whirl) and $\lambda-$ with negative frequency (backward whirl) are plotted versus Ω in the appendix, along with other plots that show some interesting symmetries in the whirl frequencies and damping. It is shown there that a plot of log (Im ($\lambda+$)) and log ($|Im$ ($\lambda-$)|) has a symmetry not revealed by a linear plot. Furthermore the loci of $\lambda+$ and $\lambda-$ in the complex plane with Im ($\lambda+$) and $|Im$ ($\lambda-$)| plotted on a log scale show more clearly how the eigenvalues are affected by the control law modifications discussed below. Such a plot of the solutions of equation (3) is shown in figure 1 for $\zeta = 0.05$. In all eigenvalue plots we are plotting the real and imaginary parts of λ, a non-dimensional quantity. The axes of the plots should strictly be labeled "Non-Dimensional Growth Rate" and "Non-Dimensional Frequency," but we use "Growth Rate" and "Frequency" for simplicity. Note that the values of Ω run up to 100, which, for $\omega_0 = 2\pi*50$ Hz and $I_p/I_t = 0.8$, corresponds to a speed of 375,000 rpm, or for $I_p/I_t = 1.2$ to a speed of 250,000 rpm. Few flywheels run to such speeds; the large range is chosen to clearly show the asymptotic behavior. (Points are plotted for Ω = (0, 0.333, and 0.666) and for $\Omega = 100^{(n/10)}$, $n = 0, 1, \ldots, 20$, in order to give roughly even point spacing on the log scale.) Note that the eigenvalue for $\Omega = 0$ is $\sim (-\zeta, 1)$, the point plotted in green. As shaft speed increases from zero, the non-dimensional forward-whirl frequency increases from 1 and the backward decreases from the same value. (We henceforth speak of the backward-whirl frequency as a positive number.) As noted in the appendix, the forward-whirl eigenvalues appear to have higher damping than the backward. However, this is true only in the sense that their growth rate has a more negative value, reflecting their higher frequencies. When the real part of the eigenvalues are divided by the frequency (absolute value of the imaginary part), the two branches of the eigenvalue plot reveal the same damping ratio (or damping factor, loss factor or percent of critical damping).
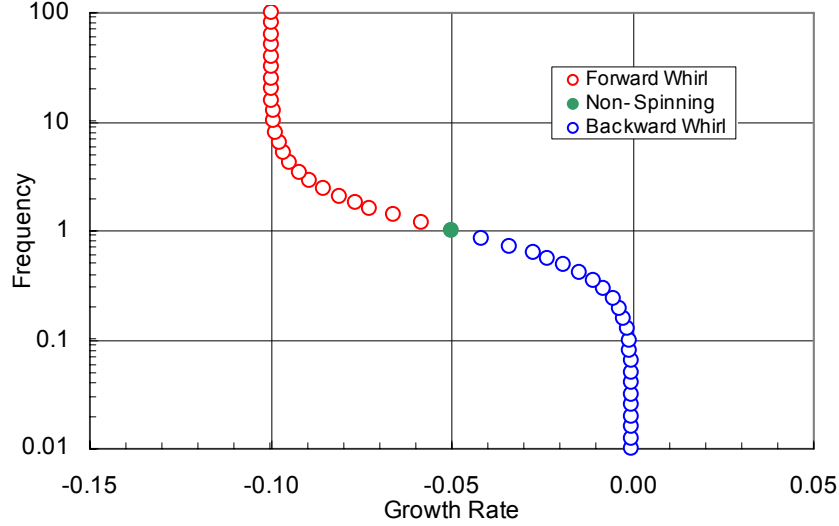
Figure 1.—Non-dimensional eigenvalue loci for $\zeta = 0.05$ and Ω values from 0 to 100. The non-spinning eigenvalue (for $\Omega = 0$) is shown in green. Forward-whirl eigenvalues are shown in red and backward-whirl eigenvalues in blue. $\Omega = 0$, 0.333, and 0.666 and $100^{(n/10)}$, for $n = 0, 1, \ldots, 20$.

B. Infinite Bandwidth with Cross-Axis Gains

Now we introduce a cross-axis gain g_{ca} into the controller so that the differential equation for shaft tilt motion becomes

$$d^2r/dt^2 + i\Omega' I_p/I_t \, dr/dt + 2\zeta\omega_0 \, dr/dt + \omega_0^2 r + i\Omega'(I_p/I_t)g_{ca}r = 0 \qquad (4)$$

where we have inserted the cross-axis term with the same sign as the gyroscopic term. We have also chosen to explicitly insert the factor Ω' (I_p/I_t) in the cross-axis term, since the gyroscopic term contains that same factor. The characteristic equation becomes (after non-dimensionalizing, as before)

$$\lambda^2 + i\Omega\lambda + 2\zeta\lambda + 1 + i\Omega g_{ca} = 0 \qquad (5)$$

The resulting eigenvalues for $\zeta = 0.05$, $\Omega = 100^{(n/10)}$, $n = 0, 1, \ldots, 10$ and for $g_{ca} = -0.025$, 0.0, and 0.025 are shown in figure 2. One can see that a positive value of g_{ca} improves backward-whirl stability but degrades forward-whirl stability. Conversely a negative value of g_{ca} improves forward-whirl stability but degrades backward-whirl stability. Note that $g_{ca} = \zeta$ gives uniform values of growth rate ($= -\zeta$) for all Ω.

To improve the stability of both modes, we can provide two cross-axis terms, corresponding to two separate parallel paths through the controller. In one path through the controller we place a forward-whirl cross-axis gain, g_f, an explicit negative sign, and a first-order high-pass filter. In a second path we place a backward-whirl cross-axis gain, g_b, an explicit positive sign, and a first-order low-pass filter. We choose the non-spinning tilt frequency as the corner frequency of both filters. The characteristic equation in this case becomes

$$\lambda^2 + i\Omega\lambda + 2\zeta\lambda + 1 + i\Omega g_b/(1+\lambda) - i\Omega g_f \lambda/(1+\lambda) = 0 \qquad (6)$$

where g_f, a positive number, is the gain that improves forward-whirl stability and g_b, also a positive number, is the gain that improves backward-whirl stability. (We have changed the sign of the forward-whirl stabilizing term to allow both gains to have positive values.) The resulting eigenvalues for $g_f = g_b = 0.025$, $\zeta = 0.05$, $\Omega = 100^{(n/10)}$, $n = 0, 1, \ldots, 10$, and $\Omega = 0$, 0.333, and 0.666 are shown in figure 3 along with the eigenvalues for $g_f = g_b = 0$. Note that in the high-speed regions the damping of each mode has been improved by the value of the cross-axis gain. There are other branches of eigenvalues (introduced by the filters) with considerably higher damping. We do not plot those. For more extreme selections of the various gains, these branches can become less stable and must be reckoned with. It is seen that with low- and high-pass filters, the stability of both forward-whirl and backward-whirl modes can be improved, as indicated by the filled symbols in figure 3.
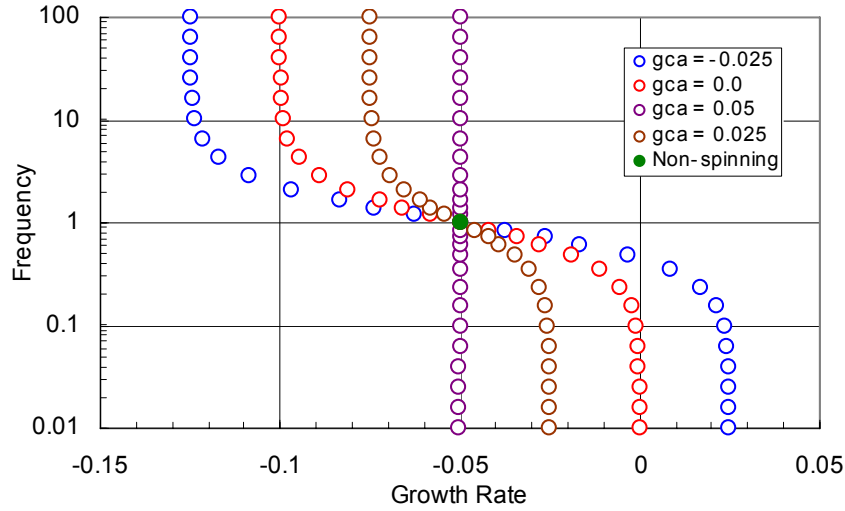
Figure 2.—Effect of Cross-Axis Gain. Positive gain improves stability of backward whirl but reduces stability of forward-whirl. $\zeta = 0.05$. $\Omega = 0$, 0.333, 0.666 and $100^{(n/10)}$, for $n = 0, 1, \ldots, 10$.
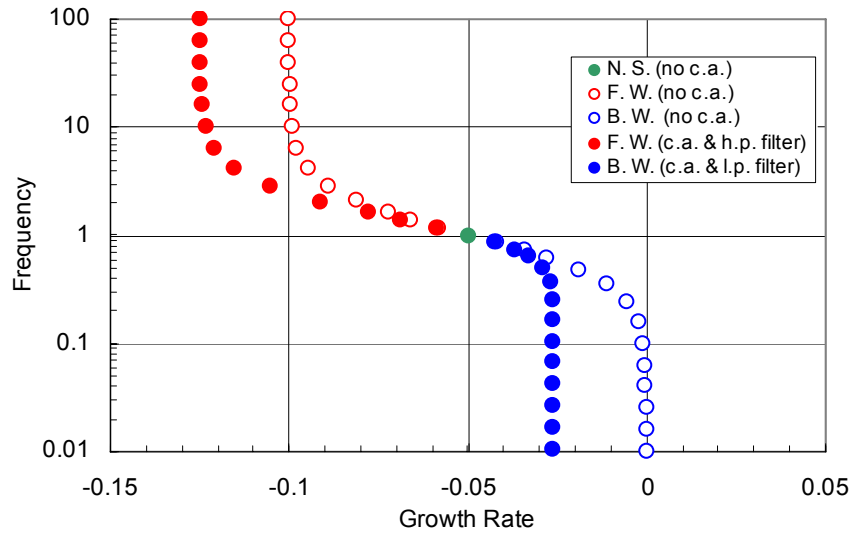

Figure 3.—Effect of High- and Low-Passed Cross-Axis Proportional Gains. Open points are for cross axis (c.a.) gains equal to 0. Filled points are for $g_f = g_b = 0.025$ and $\zeta = 0.05$.

C. Effect of Finite Bandwidth with Filtered Cross-Axis Gains

The appendix lists a number of sources of delays and phase lags that are typically found in a digitally controlled magnetic bearing system. We now consider the effect of these destabilizing influences. To qualitatively explore these influences, we arbitrarily pick 5 first-order filters, in series in the closed control loop, and all with the same corner angular frequency, ω_c, measured in units of ω_0. Thus every term in the controller is considered to be multiplied by the following factor, f:

$$f \equiv 1/\left(1 + \lambda/\omega_c\right)^5 \tag{7}$$

The characteristic equation becomes

$$\lambda^2 + i\Omega\lambda + f\left[1 + 2\zeta\lambda + i\Omega g_b/(1+\lambda) - i\Omega g_f\lambda/(1+\lambda)\right] = 0 \qquad (8)$$

Some representative solutions for various values of ω_c are shown in figure 4. We now plot values of Ω ranging only up to 40, which, if the non-spinning tilt mode is set at 50 Hz, would represent a shaft speed of 150,000 rpm for $I_p/I_t = 0.8$ or 100,000 rpm for $I_p/I_t = 1.2$. The points for $\omega_c = 800,000$ (effectively an infinite bandwidth, since ω_c is measured in units of ω_0) are for the same gains as the filtered cases plotted in figure 3. The value of $\omega_c = 80$ yields a total phase lag around the closed loop of about 70° at 1 kHz (for our usual example with $\omega_0 = 314$ rad/sec (50 Hz)). This is close to the phase lag at 1 kHz in the actual system described in reference 4. Note that the forward-whirl mode becomes unstable at about $\Omega = 20$, or 75,000 rpm for $I_p/I_t = 0.8$ or 50,000 rpm for $I_p/I_t = 1.2$. Note that even the damping of the non-spinning tilt mode is reduced by more than half by the filters.

Examine now to what extent increasing the tilt damping constant ζ can improve the stability of the forward-whirl mode. In figure 5, we show the eigenvalues for 3 values of ζ, namely $\zeta = 0.025$, 0.05, and 0.075. We see that higher tilt damping ζ improves the forward-whirl stability until the frequency of the mode is somewhat over 20. Then more tilt damping is actually destabilizing.
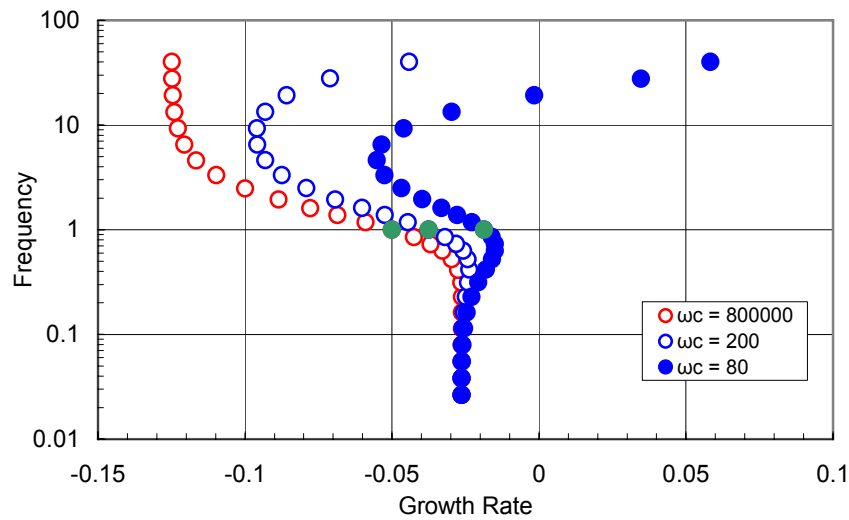

Figure 4.—Effect of Finite Bandwidth on Eigenvalues. $\Omega = 0.333$, 0.666 and $40^{(n/10)}$, $n = 0, 1, \ldots, 10$. $g_f = g_b = 0.025$, $\zeta = 0.05$.
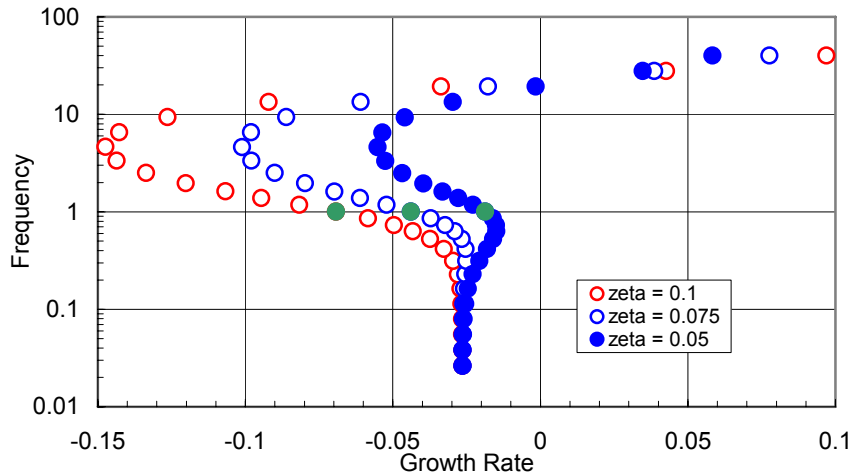

Figure 5.—Effect of zeta on forward-whirl eigenvalues at high speed. Higher zeta improves forward stability up to about $\Omega = 20$. $g_f = g_b = 0.025$. $\omega_c = 80$.

Consider now whether higher forward-whirl cross-axis proportional gain can help. Eigenvalues are shown in figure 6 for $\zeta = 0.05$ and $g_b = 0.025$ for three values of g_f, namely (0.025, 0.05, and 0.075). Higher values of g_f improve the stability of the forward whirl mode for lower speeds, but the same "barrier" appears at about the same frequency. The reason for this becomes clear from a look at the phase lag of the filter function f as a function of frequency, plotted in figure 7. We see that at a non-dimensional frequency of about 26, the phase lag is 90°. Damping can advance phase by at most 90°, so when the non-dimensional forward-whirl frequency reaches 26, the beneficial phase advance desired from damping is entirely obliterated by the system phase lag. But we can counteract the phase lags beyond this point with a phasor advance, as we now show.
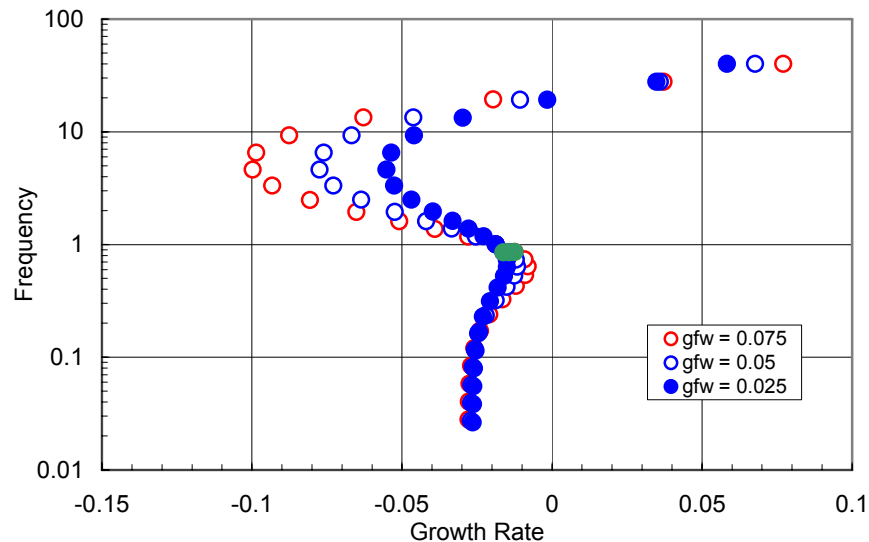
Figure 6.—Effect of forward-whirl cross-axis gain on eigenvalues with significant phase lags present. $g_b = 0.025$, $\zeta = 0.025$, $\omega_c = 80$.
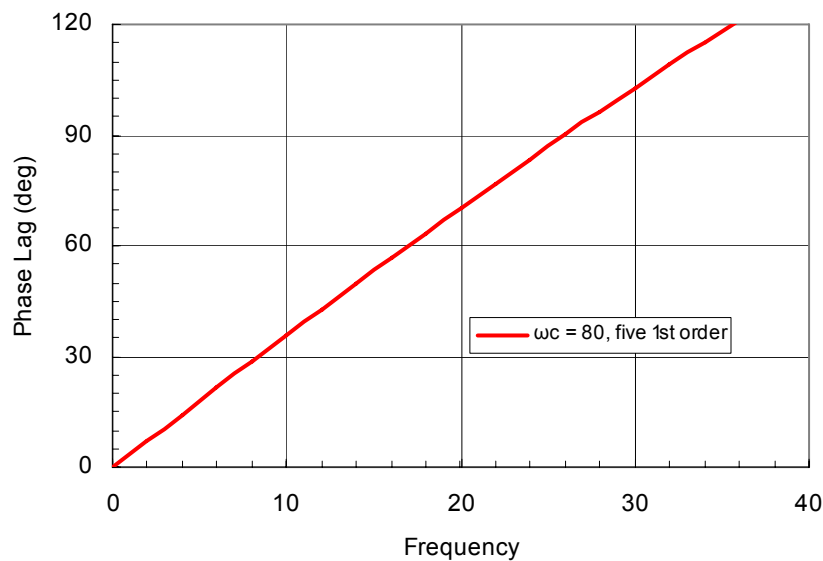

Figure 7.—Phase lag in closed-loop as a function of frequency. Product of five first order filters with corner non-dimensional frequencies of 80.

D. Effect of Phasor Advance with Finite Bandwidth and Filtered Cross-Axis Gains

Now consider trying to counteract the phase lags discussed in the last section. If we multiplied the cross-axis term in the controller that contains the high-pass filter by a phasor, p, of unit magnitude, defined by

$$p \equiv \exp\left\{-iArg\left[1/\left(1-i\Omega/\omega_c\right)^{npoles}\right]\right\} \tag{9}$$

where *npoles* is the order of the filter, then we would expect to approximately counteract the system phase lags. An adequate approximation of equation (9) for high shaft speed is

$$p \approx \exp\left[-i(\pi/4)(\Omega/\omega_c)npoles\right] \tag{10}$$

For $\Omega \gg 1$ this gives an approximation of the phase lags caused by the function *f*. That is, at high shaft speed, for which the forward-whirl frequency is asymptotic to Ω, this approximately nullifies the phase lags introduced by the function *f*, at least as far as the forward-whirl cross-axis feedback term is concerned. The characteristic equation then becomes

$$\lambda^2 + i\Omega\lambda + f\left[1 + 2\zeta\lambda + i\Omega g_b/(1+\lambda) - ip\Omega g_f\lambda/(1+\lambda)\right] = 0 \tag{11}$$

An eigenvalue plot for this case is shown in figure 8, along with the eigenvalues for no phasor correction. A plot of just the damping of the forward-whirl mode as a function of Ω is shown in figure 9. Inspection of the figures 8 and 9 reveals that applying the phase correction gives little change in stability for Ω less than 10, but an increasing improvement at higher speed, raising the instability speed from 22 to 35 (which, for our example with the non-spinning tilt frequency set at 50 Hz, would be from 82,500 rpm to 131,250 rpm for $I_p/I_t = 0.8$ or from 55,000 rpm to 87,500 rpm for $I_p/I_t = 1.2$). However, as shown in figure 10, the magnitude of the filter f falls substantially below 1 as Ω approaches 40. Therefore, a magnitude correction for the effect of the filter function *f* is warranted. We therefore replace equation (10) by

$$p \equiv M \exp\left(-i(\pi/4)(\Omega/\omega_c)npoles\right) \tag{12}$$

where

$$M \equiv abs\left(1/(1+i(\Omega/\omega_c))^{npoles}\right) \tag{13}$$

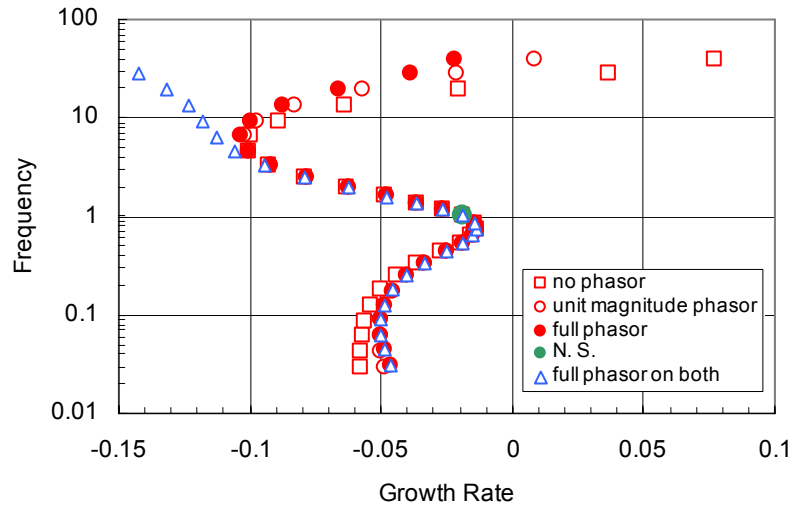
Figure 8.—Effect of phasor corrections for system filters. $g_f = 0.075$, $g_b = 0.5$, $\zeta = 0.05$, $\omega_c = 80$. Phasor applied to forward-whirl term only—red circles. Full phasor applied to both forward-whirl and damping term—blue triangles.
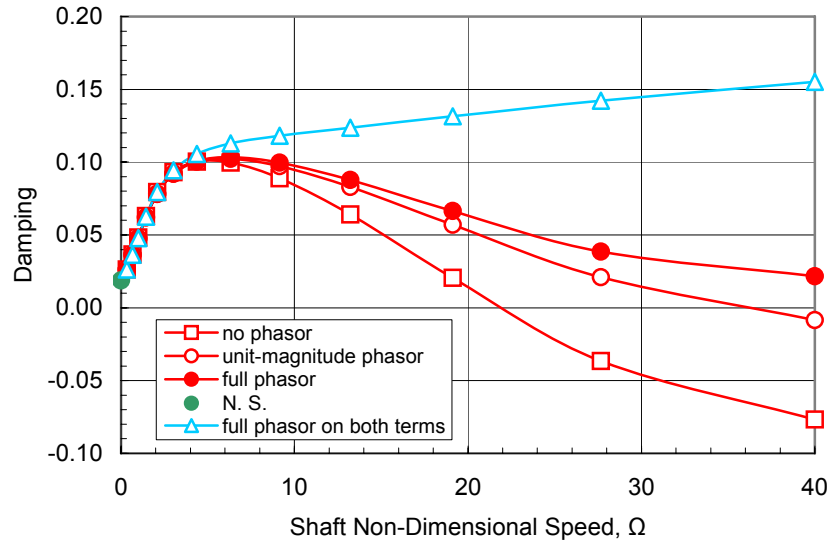
Figure 9.—Damping as a function of shaft non-dimensional speed for various phasor corrections. $g_f = 0.075$, $g_b = 0.5$, $\zeta = 0.05$, $\omega_c = 80$. Phasor applied to damping term only—red symbols. Squares—no phasor. Open circles—unit-magnitude phasor. Closed circles—full phasor. Blue triangles—full phasor applied to both forward-whirl and damping terms.
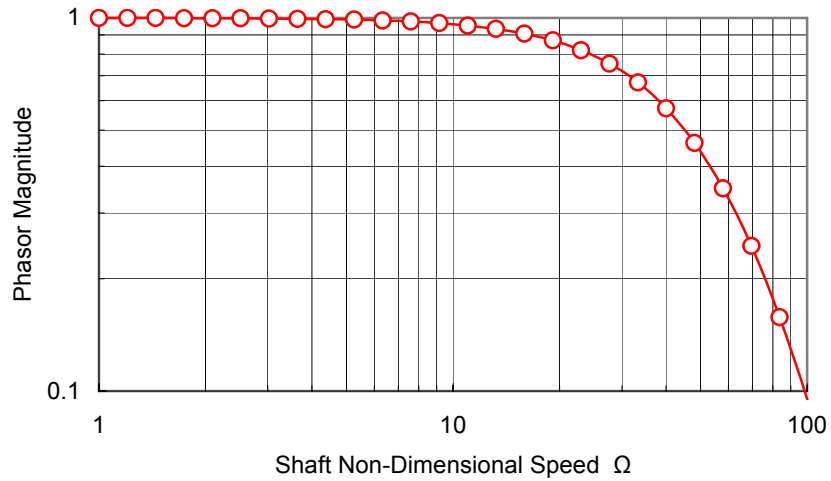

Figure 10.—Magnitude of assumed lumped filters in magnetic bearing closed loop. The magnitude M of the phasor is plotted. $\omega_c = 80$.

In figures 8 and 9, it can be seen that the magnitude correction provides an increasing benefit with speed above about $\Omega = 6$. Next consider the effect of applying the phasor correction to the term in equation (11) that contains zeta (which came from the first derivative term in the differential equation), rather than to the forward-whirl term. The characteristic equation then becomes

$$\lambda^2 + i\Omega\lambda + f\left(1 + 2p\zeta\lambda + i\Omega g_b/(1+\lambda) - i\Omega g_f\lambda/(1+\lambda)\right) = 0 \tag{14}$$
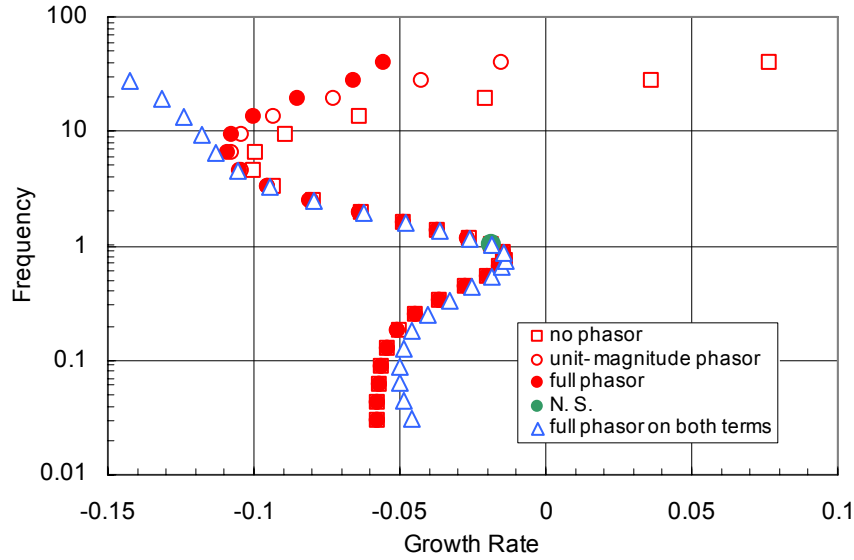
Figure 11.—Eigenvalues with phasor correction applied to derivative term and to both derivative and forward-whirl terms. $g_f = 0.075$, $g_b = 0.5$, $\zeta = 0.05$, $\omega_c = 80$.

The eigenvalues for this case are shown in figure 11 for the case where M is given by equation (13) (full phasor) and the case where M is set equal to 1 (phase correction only). Comparison of figures 10 and 11 indicates that a greater stability benefit is obtained by correcting the phase lag of the derivative term than by correcting the phase lag of the forward-whirl term, at least for the values of the other parameters used here. Correcting both has a still larger benefit, as is shown in figures 10 and 11 by the points plotted in blue. However, it should be remembered that the use of the derivative term entails noise amplification.

E. Removal of Derivative Feedback at High Shaft Speed

In figure 12 we plot the forward whirl eigenvalues (in open blue triangles, as in figs. 8 and 11, and using the same data as in those figures) that result from applying the full phasor correction, equations (12) and (13), to both the forward-whirl feedback term and the damping term, and the eigenvalues (in open orange symbols) with the full phasor correction applied to the forward-whirl term but with the damping constant ζ set equal to zero. It can be seen that above a non-dimensional speed of 3, the system is stable with $\zeta = 0$. Thus we can expect that a transition from the open orange eigenvalues at low speed to the open blue eigenvalues at high speed would yield the benefit of stability at all speeds, but low noise generation at high speed where the system may be more vulnerable. As one illustration of this approach we choose to gain schedule the value of ζ in the following manner:

$$\zeta = \zeta_0 / \left(1 + (\Omega/\Omega_0)^n \right) \tag{15}$$

where ζ_0 is the initial value of ζ, Ω_0 sets the shaft speed around which the transition to $\zeta = 0$ takes place, and the exponent n governs the rapidity of the transition. As a specific example, plotted with filled red symbols in figure 12, we choose $\zeta_0 = 0.05$, $\Omega_0 = 8$, and $n = 4$. The transition between the limiting loci in blue and orange is clearly seen.
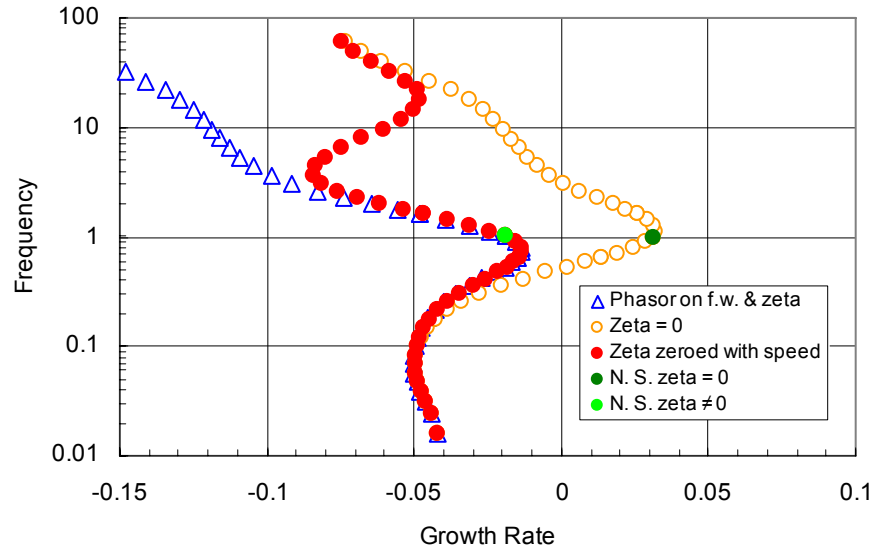
Figure 12.—Removal of damping feedback at high speed. Blue triangles—full phasor advance applied to both forward-whirl and damping terms with $g_f = 0.075$, $g_b = 0.5$, $\omega_c = 8$, $\zeta = 0.05$; orange circles—$g_f = 0.075$, $g_b = 0.5$, $\omega_c = 80$, $\zeta = 0$; Red circles—transition from $\zeta = 0.05$ to $\zeta = 0.0$ according to equation (15).

III. Experimental Use of Methods

The effectiveness of cross-axis proportional gains was experimentally demonstrated (ref. 4) on the "D1" energy storage flywheel unit (with $I_p/I_t = 0.8$) at Glenn at speeds up to 60,000 rpm and on predecessor flywheels. The qualitative effect of a single unfiltered cross-axis gain on forward-and backward whirl stability was easily seen by measuring the spectral density versus frequency of the position sensor signals. When the controller was of the type described by equations (4) and (5), one sign of g_{ca} raised the amplitude of the forward whirl peak in the spectral density and reduced the backward whirl peak. The opposite sign of g_{ca} had the opposite effect. The sharpening of each peak in turn was useful for accurate frequency measurements of the whirl modes.

Filtered cross-axis gains, described by equation (6), had the predicted qualitative effect of reducing the spectral density peaks of both the forward and backward whirl modes.

The phase advance method described by equations (10) to (14) was applied in a limited sense. Rather than attempting to use the full angular advance of equation (10), smaller angular advances were applied to the forward whirl controller term and/or to the controller's damping term while the forward-whirl peak in the sensor spectral density was monitored. The advance was beneficial, but only enough advance was applied to render the peak size non-threatening. The magnitude correction of equations (12) and (13) was not attempted. The elimination of the damping term described at high shaft speed described by equation (15) has not been implemented. The reason for caution in applying these latter methods stems from the omission of flexible modes from the present analysis. The inclusion of these modes is beyond the intended scope of our analysis. However the flywheel of reference 4 had a flexible mode which was actually crossed by the synchronous shaft speed near the maximum design speed. Thus we could not expect the present analysis to adequately describe the system stability in that speed range.

IV. Concluding Remarks

We have approached the control of gyroscopic modes of a high-speed flywheel from the standpoint of classical control theory. We have assumed the use of a centralized modal controller that allows us to work with the tilt modes only, excluding motions not affected by gyroscopic influences. We have excluded flexible modes from the discussion. We have desired to get as simple and physical an understanding of the modal behavior and the effects of the various control approaches as possible. We have been motivated to produce a control strategy that generates low noise in the closed loop. A modern control approach could achieve this as well, but with less transparency.

Stability of both forward- and backward-whirl modes was shown to be improved by the use of cross-axis proportional gains, aided by high- and low-pass filters that permit the controller to affect the modes independently when the rotor speed is high. The forward-whirl mode stability was seen to be degraded at high rotor speed by system phase lags, because the forward-whirl frequency increases indefinitely with rotor speed. It was shown that the severity of the stability reduction can be reduced by applying a phasor advance in the controller to counteract the system phase lags. Lastly it was shown that the tilt damping feedback in the controller could be entirely removed at a sufficiently high shaft speed.

Appendix

A. Relation between Forward- and Backward-Whirl Eigenvalues

Consider a magnetically supported flywheel with infinite bandwidth in its closed-loop control system. The eigenvalues of the system are the solutions of equation (3). The imaginary parts of the solutions to equation (3) for $\Omega \neq 0$ have two signs. A plot of these eigenvalues on linear scales is shown in figure A1. The limits of the two solutions for $\Omega \rightarrow 0$ are $(-\zeta \pm i)$, plotted in figure A1 as the two green points. (Note that $\zeta = 0.05$ for this case.) As Ω increases, the forward-whirl frequency increases and the backward-whirl frequency, which has a negative value, decreases in magnitude. A plot of the eigenvalues with the frequency replaced by its absolute value is shown in figure A2, which gives a slightly better picture of modes developing from a common single non-spinning frequency. But the most illuminating plot of the eigenvalues is one in which the absolute value of the frequency is plotted on a logarithmic scale, as in figure A3. This reveals a symmetry that might have been unsuspected. The product of the absolute values of the frequencies is approximately constant and the sum of the absolute damping values (negative of the growth rates) is fixed. The absolute values of the frequencies of the two modes are plotted as a function of the spinning speed in figure A4. Now consider figure A3 again. It appears from the figure that the forward-whirl modes are better damped than the backward. This is true in the sense that they damp out faster in time; the absolute damping is higher. However, if the real part of each eigenvalue in figure 3 is divided by the absolute value of the imaginary part to obtain the fraction of critical damping, then the curve of figure A5 is obtained. See that the two modes are equally damped as a fraction of critical damping, that is, the amplitudes of forward and backward-whirl oscillations, initiated by some disturbance, will decay to a given fraction of their initial amplitudes in the same number of cycles. However, the elapsed time for decay to a given fraction of initial amplitude is shorter for forward whirl than for backward whirl.

B. Sources of Phase Lags and Delays in Magnetic-Bearing-Supported Flywheel Systems

Every component in a closed loop magnetic bearing system has a bandwidth which limits the high-frequency response of the system and introduces phase lags. These phase lags may not severely affect rigid-rotor backward whirl because of the low frequency of those modes. However, the frequency of the forward-whirl mode is asymptotic to $(I_p/I_t) * \Omega'$, and therefore may be on the order of a kilohertz for high speed
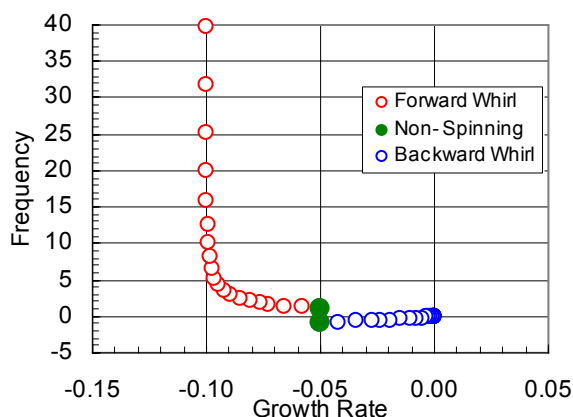

Figure A1.—Eigenvalues of equation (3), plotted without any alteration. $\Omega = 0$, 0.333, 0.666 and $100^{(n/20)}$, $n = 0, 1, \ldots, 16$.
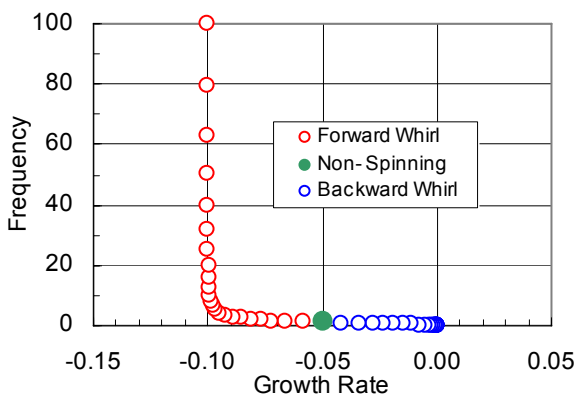

Figure A2.—Eigenvalues of equation (3), plotted using absolute values of imaginary parts. $\Omega = (0, 0.333, 0.666)$ and $100^{(n/20)}$, $n = 0, 1, \ldots, 20$.
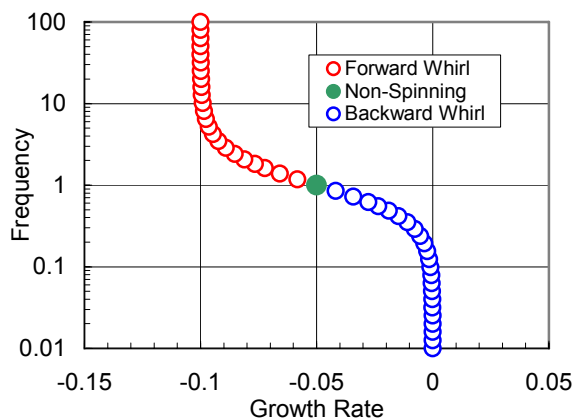

Figure A3.—Eigenvalues of equation (3), with absolute values of frequencies plotted on log scale. $\Omega = (0, 0.333, 0.666)$ and $100^{(n/20)}$, $n = 0, 1, \ldots, 20$.

energy storage flywheels. Phase lags of several components can be appreciable at such a frequency and lead to forward-whirl instability. The sources of phase lag or delay include the following:

(1) The lowest bandwidth in a magnetic bearing system is often that of the power amplifiers, which are commonly configured as transconductance amplifiers (voltage command input, current output), in combination with their inductive load. This bandwidth is usually only one or two kilohertz or less. We pick 2 kHz for definiteness here, with a phase lag of the order of 22° at 1 kHz.

(2) A digital controller implemented on a digital signal processor (DSP) can introduce serious phase lags. One of these (sometimes worse than the power amplifiers) comes from the anti-aliasing input filter in front of the processor that runs the control code. If the sample rate is 25,000/sec, the filter is usually set to cut off frequencies above the Nyquist frequency of 12.5 kHz. The filter may be 6th order and produce a phase lag of the order of 30° at 1 kHz.

(3) A digital signal processor board can also have a smoothing filter on the output that produces as much phase lag as the input filter. We suppose for this paper that there is only a first order filter at the Nyquist frequency of 12.5 kHz, giving a phase lag at 1 kHz of about 4°.

(4) The sampling itself introduces a low-pass filtering effect with a corner at the Nyquist frequency. This gives about 5° at 1 kHz for a 25 kHz sampling rate.

(5) Another lag, distinct from the sampling lag, is the latency delay in the controller. A signal introduced at the input (after the anti-aliasing filter) and sent directly to the output (before the smoothing filter) arrives there after some elapsed time, which is often on the order of the time between samples, but can be worse by the amounts of input and output settling times. This might add another 5° of lag at 1 kHz.

(6) Another lag is due to eddy currents in the magnetic bearings. The magnetic field in the working gap lags behind the current in the windings by an amount that depends on the size of the bearing poles and the thickness of the laminations (mainly the latter). It can contribute 10 to 20° phase lag at 1 kHz.

(7) The last obvious component that can introduce phase lag is the position sensor. In most cases the bandwidth of a sensor is 20 kHz or better, yielding no more than a degree or two phase lag at 1 kHz.

To bring out general principles in this non-dimensional study without having to be specific on these phase lags, we lump all the filtering effects into a simple product of first order filters. We use a product of five first order filters, all with the same corner frequency, and measure that frequency in units of ω_0, as is done with all frequencies.
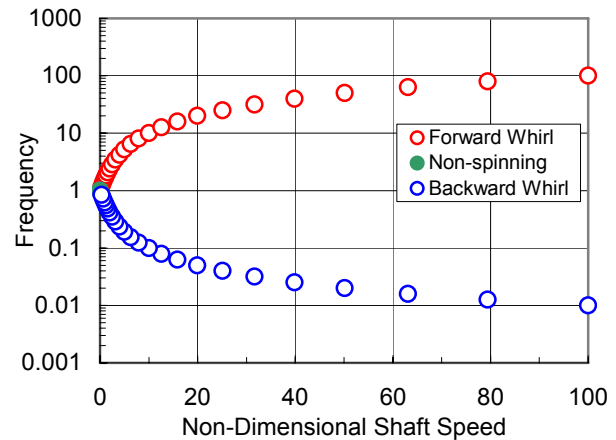

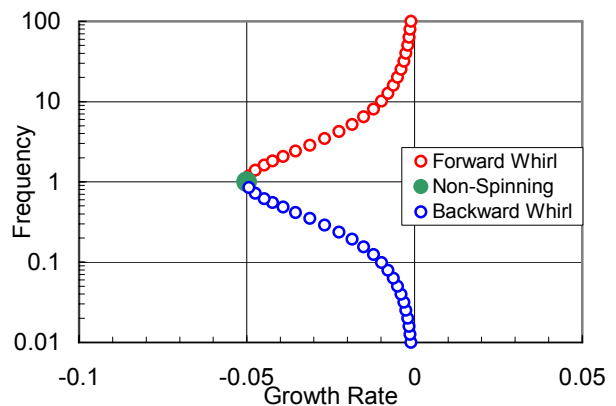Figure A4.—Frequencies of forward- and backward-whirl as functions of the non-dimensional spinning speed.

Figure A5.—Eigenvalues with real parts plotted in terms of fraction of critical damping. $\Omega = (0, 0.333, 0.666)$ and $100^{(n/20)}$, n = 0, 1, …, 100.

TABLE I.—EXAMPLE PHASE LAGS IN A
MAGNETIC-BEARING-SUPPORTED FLYWHEEL SYSTEM.

Delay Source	Phase Lag @ 1 kHz
Power amplifiers (1st order @ 2 kHz)	22
Anti-alias filter (6th order @ 12.5 kHz)	24
Smoothing filter (1st order @ 12.5 kHz)	4
Sampling @ 25 kHz	5
Latency @ 25 kHz	5
Magnetic core eddy currents	10
Position sensors	1
Total phase lag @ 1 kHz	71

For a 25 kHz sampling rate, the above listed phase lags add up to 71° at 1 kHz. A product of five first-order filters will produce approximately that phase lag if the corner frequency ω_c is set at about 4 kHz. For a 60,000 rpm (1000 Hz) flywheel this is 4 times the spinning frequency. In terms of an assumed non-spinning tilt frequency of 50 Hz, the value of ω_c would be 80. In the main text a number of results are presented for $\omega_c = 80$.

References

1. Ahrens, M., Kucera, L. and Larsonneur, R.: "Performance of a Magnetically Suspended Flywheel Energy Storage Device," IEEE Transactions on Control Systems Technology, vol. 4, no. 5, September 1996.
2. Vance, J.M., Rotordynamics of Turbomachinery, John Wiley & Sons, New York, 1988, pg. 125.
3. Kascak, A.F., "Stability Limits of a PD Controller for a Flywheel Supported on Rigid Rotor and Magnetic Bearings," AIAA Guidance, Navigation and Controls Conference, San Francisco, CA, 2005, AIAA–2005–5956.
4. Dever, T.P., Brown, G.V., Duffy, K.P., and Jansen, R.H.: "Modeling and Development of a Magnetic Bearing Controller for a High Speed Flywheel System," Second International Energy Conversion Engineering Conference, Providence, RI, Aug. 16–19, 2004, paper no. AIAA–2004–5626.

REPORT DOCUMENTATION PAGE

1. AGENCY USE ONLY (Leave blank)	2. REPORT DATE	3. REPORT TYPE AND DATES COVERED
	January 2006	Technical Memorandum

4. TITLE AND SUBTITLE

Stabilizing Gyroscopic Modes in Magnetic-Bearing-Supported Flywheels by Using Cross-Axis Proportional Gains

5. FUNDING NUMBERS

WBS 561581.02.08.03
1L161102AF20

6. AUTHOR(S)

Gerald V. Brown, Albert F. Kascak, Ralph H. Jansen, Timothy P. Dever, and Kirsten P. Duffy

7. PERFORMING ORGANIZATION NAME(S) AND ADDRESS(ES)

National Aeronautics and Space Administration
John H. Glenn Research Center at Lewis Field
Cleveland, Ohio 44135–3191

8. PERFORMING ORGANIZATION REPORT NUMBER

E–15382

9. SPONSORING/MONITORING AGENCY NAME(S) AND ADDRESS(ES)

National Aeronautics and Space Administration
Washington, DC 20546–0001
and
U.S. Army Research Laboratory
Adelphi, Maryland 20783–1145

10. SPONSORING/MONITORING AGENCY REPORT NUMBER

NASA TM—2006-214027
ARL–TR–3799
AIAA–2005–5955

11. SUPPLEMENTARY NOTES

12a. DISTRIBUTION/AVAILABILITY STATEMENT

Unclassified - Unlimited
Subject Category: 37

Available electronically at http://gltrs.grc.nasa.gov

This publication is available from the NASA Center for AeroSpace Information, 301–621–0390.

12b. DISTRIBUTION CODE

13. ABSTRACT *(Maximum 200 words)*

For magnetic-bearing-supported high-speed rotating machines with significant gyroscopic effects, it is necessary to stabilize forward and backward tilt whirling modes. Instability or low damping of these modes can prevent the attainment of desired shaft speed. We show analytically that both modes can be stabilized by using cross-axis proportional gains and high- and low- pass filters in the magnetic bearing controller. Furthermore, at high shaft speeds, where system phase lags degrade the stability of the forward-whirl mode, a phasor advance of the control signal can partially counteract the phase lag. In some range of high shaft speed, the derivative gain for the tilt modes (essential for stability for slowly rotating shafts) can be removed entirely. We show analytically how the tilt eigenvalues depend on shaft speed and on various controller feedback parameters.

14. SUBJECT TERMS

Flywheels; Magnetic bearings; Gyroscopic; Energy storage

15. NUMBER OF PAGES

21

16. PRICE CODE

17. SECURITY CLASSIFICATION OF REPORT	18. SECURITY CLASSIFICATION OF THIS PAGE	19. SECURITY CLASSIFICATION OF ABSTRACT	20. LIMITATION OF ABSTRACT
Unclassified	Unclassified	Unclassified	